第 32卷 第 2期　　焊　接　学　报　　Vol.32　No.2
2011年 2月　　TRANSACTIONS OF THE CHINA WELDING INSTITUTION　　February　2011

双相钢点焊熔核界面撕裂失效模式评价

杨海军[1]，　张延松[1]，　来新民[1]，　张小云[2]
（1. 上海交通大学 机械与动力工程学院，上海　200240；
2. 上海通用汽车有限公司 整车制造工程部，上海　201201）

杨海军

摘　要：双相钢点焊熔核中大量的相变马氏体，导致熔核脆性增加，其界面撕裂问题严重降低了焊点的力学性能，导致接头质量下降。采用传统的评价标准会产生焊点界面撕裂问题。针对双相钢焊点界面撕裂评价问题，建立了基于焊点宏观形貌与微观特征的双相钢焊点失效模式评价模型，获得了双相钢焊点界面撕裂的临界熔核直径评价标准，最后在 1.4，1.8 mm厚 DP600钢板上通过试验验证。结果表明，临界熔核直径评价标准克服了传统经验公式及现有评价标准考虑因素不全的缺点，成功地实现了双相钢焊点失效模式的准确评价。

关键词：双相钢；电阻点焊；界面撕裂；评价模型
中图分类号：TG438　　文献标识码：A　　文章编号：0253－360X(2011)02－0061－04

0　序　　言

随着全球能源与环境危机的日益加重，节能减排成为汽车设计制造面临的严峻课题。研究表明，燃油消耗的 50 %是由于汽车的重量引起的[1]，因此，减少汽车自身重量是节能减排的有效措施。降低车重最有效的方法之一是使用轻质高强钢，其典型代表双相钢（DP）凭借自身优点目前已经成为车身制造中应用前景最广泛的一种高强钢材料[2]。双相钢的使用在降低车重的同时，也给车身电阻点焊装配带来了挑战：由于双相钢本身结构特点，点焊时会形成大量的相变马氏体，从而导致熔核脆性增加，在进行焊点力学性能测试时，除了传统的熔核剥离模式（button pull-out）外，还容易产生从熔核界面撕裂（interfacial fracture）现象，严重降低了焊点的力学性能[3]。

研究表明，对于双相钢而言，传统的熔核直径仍会产生焊点界面撕裂问题，需要新的熔核直径评价标准。文献[4－6]分别通过试验推导了双相钢焊点避免界面撕裂模式的最小熔核直径，但这些公式由于考虑因素不全面，在评价不同板厚与等级的双相钢焊点失效模式时，精度较差。

文中以车身应用最广泛的双相钢 DP600为例，针对焊点力学性能测试中普遍采用的拉剪模式，考虑焊点宏观压痕和微观维氏硬度，对双相钢焊点进行力学建模分析，根据两种不同失效模式（界面撕裂和熔核剥离）下焊点失效区应力分布，计算其所能承受的最大载荷，从而获得评价焊点失效模式的临界熔核直径指标，最后以 1.4，1.8 mm两种不同厚度的双相钢 DP600为例，通过试验测定不同失效模式下的熔核宏观及微观参数，对理论推导结果进行验证。

1　不同失效模式的焊点受载分析

1.1　界面撕裂模式下的焊点受载

如图 1所示，将焊点假设为圆柱体，在进行拉剪试验时，熔核区承受切向剪应力，假设熔核直径为 d，半径为 r，熔核区厚度为 $2t_N$（thickness of nugget），所受拉剪力为 F_{shear}。

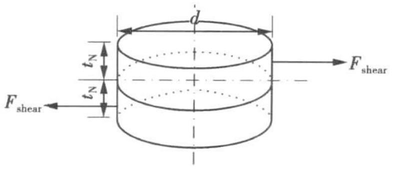

图 1　熔核界面撕裂受力模型
Fig. 1　Model for interfacial fracture of nugget

收稿日期：2009－06－01
基金项目：国家自然科学基金资助项目（50905111）；上海汽车工业科技发展基金资助项目（0907）

发生焊点界面撕裂模式时，熔核界面剪应力 τ 达到最大承受极限 $\tau_{\max}$。此时，假设熔核内部组织均匀，纯拉剪状态焊点界面剪应力分布为从熔核中心到边缘呈线性[7]，如图 2所示.

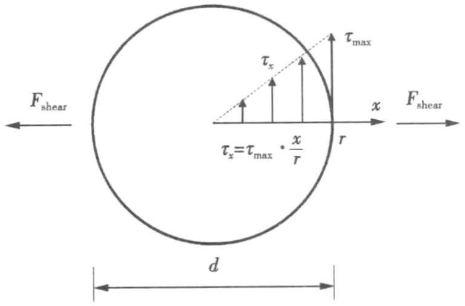

(a) 剪应力值变化示意图

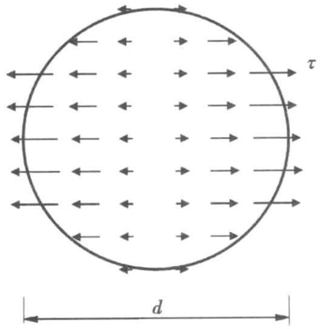

(b) 剪应力分布图

图 2 焊点界面撕裂剪应力分布

Fig. 2 Shear stress distribution of nugget under interfacial fracture mode

则剪应力 τ 是位置 x 的函数，即

$$\tau_x=\tau_{\max}\cdot\frac{x}{r} \tag{1}$$

位置 x 处的微分面积为：

$$ds=2\sqrt{r^2-x^2}\,dx$$

因此，发生熔核界面撕裂时，焊点所能承受的最大拉剪力为

$$F_{IF}=\int\tau_x\,ds=\int_0^r\tau_{\max}\cdot\frac{x}{r}\cdot 2\sqrt{r^2-x^2}\,dx$$

$$=\frac{2}{3}\tau_{\max}\cdot r^2=\frac{1}{6}\tau_{\max}\cdot d^2 \tag{2}$$

式中：F_{IF} 为发生界面撕裂模式时，熔核所能承受的极限拉剪力，$\tau_{\max}$ 为发生界面撕裂时，熔核界面所能承受的极限剪应力.

1.2 熔核剥离模式下的焊点受载

当发生熔核剥离的模式时，整个熔核从母材中分离，失效位置为熔核周边热影响区，是由于该区承受的拉应力 σ 达到其所能承受的极限 $\sigma_{\max}$ 而导致失效. 此时焊点的受力模型如图 3所示，在拉剪力作用下，熔核略有变形，假设熔核厚度为 $2t_N$，熔核失效处直径为 d，受到的拉剪力为 F_{shear}.

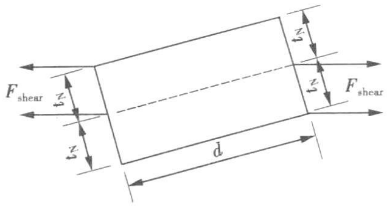

图 3 熔核剥离模型

Fig. 3 Pull-out failure model for nugget

熔核剥离模式失效区为热影响区周边，此时，该表面承受极限拉应力，参考文献[8]，其拉应力按正弦规律分布，如图 4所示.

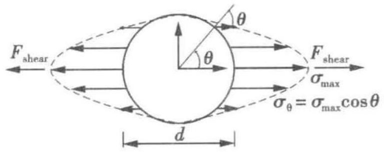

图 4 焊点熔核剥离拉应力分布

Fig. 4 Tensile stress distribution of nugget under button pullout mode

则 θ 处的拉应力 σ_θ 应为

$$\sigma_\theta=\sigma_{\max}\cos\theta \tag{3}$$

位置 θ 处的面积微分为

$$ds=r\cdot t_N\cdot d\theta$$

由于该位置截面与拉应力成 θ 角度，故该处的拉剪力微分为

$$dF_{PO}=\sigma_\theta\cdot ds\cos\theta=r\cdot t_N\cdot\sigma_{\max}\cos^2\theta\,d\theta$$

故熔核剥离失效时，其所承受的极限拉剪力为

$$F_{PO}=\int dF_{PO}=2\int_0^{\pi/2}r\cdot t_N\cdot\sigma_{\max}\cos^2\theta\,d\theta$$

$$=\frac{\pi}{2}t_N\cdot r\cdot\sigma_{\max}=\frac{\pi}{4}t_N\cdot d\cdot\sigma_{\max} \tag{4}$$

式中：F_{PO} 为发生熔核剥离模式时，熔核所能承受的最大拉剪力，$\sigma_{\max}$ 为发生熔核剥离时，熔核失效位置表面所能承受的极限拉应力.

2 临界失效模式熔核直径计算

综上所述，当双相钢焊点发生临界失效模式时，熔核所能承受的拉剪力 F_{IF} 与 F_{PO} 应相等，即

$$\frac{1}{6}\tau_{\max}\cdot d^2=\frac{\pi}{4}t_N\cdot d\,\sigma_{\max} \tag{5}$$

因高强钢发生界面撕裂时, 受剪应力作用, 失效在熔核区, 而发生熔核剥离时, 受拉应力作用, 失效在热影响区, 故由上式计算可得

$$d=1.5\pi\cdot t_N\cdot\frac{(\sigma_{\max})_{HAZ}}{(\tau_{\max})_{FZ}} \tag{6}$$

式中: $(\sigma_{\max})_{HAZ}$为热影响区极限拉应力; $(\tau_{\max})_{FZ}$为熔核区极限剪应力. 由 Tresca失效准则, 材料所能承受的极限拉应力约为极限剪应力的 2倍, 故上式可转化为

$$d=3\pi\cdot t_N\cdot\frac{(\sigma_{UTS})_{HAZ}}{(\tau_{UTS})_{FZ}} \tag{7}$$

式中: $(\sigma_{UTS})_{HAZ}$为热影响区极限拉应力; $(\tau_{UTS})_{FZ}$为熔核区极限拉应力, 根据材料的极限拉应力与维氏硬度的比例关系[9]为

$$\sigma_{UTS}=C\cdot H \tag{8}$$

式中: C为比例系数; H为材料的维氏硬度; 使用 d_{cr} (critical diameter)代替 d可得

$$d_{cr}=3\pi\cdot t_N\cdot\frac{H_{HAZ}}{H_{FZ}} \tag{9}$$

式中: H_{HAZ}为热影响区的维氏硬度; H_{FZ}为熔核区的维氏硬度. 考虑焊点压痕的作用, 假设压痕分数为 $I\%$, 即压痕深度占工件总厚度的百分比, 则

$$t_N=(1-I\%)h \tag{10}$$

可得

$$d_{cr}=3\pi\cdot(1-I\%)h\cdot\frac{H_{HAZ}}{H_{FZ}} \tag{11}$$

式中: h为板厚. 由此可知, 发生两种失效模式的临界熔核直径 d_{cr}与板厚 h, 焊点压痕分数 $I\%$, 以及熔核与热影响区的维氏硬度 H_{FZ}, H_{HAZ}有关.

3　试验结果

试验采用两种不同厚度 1.4, 1.8 mm双相钢 DP600, 其合金含量 (质量分数, %)分别为 0.12C, 2.06Mn, 0.51Si以及 0.39Cr. 焊接工艺参数选取如表 1所示.

表 1　不同厚度 DP600焊接参数选取

Table 1　Weld parameter selection for DP600 sheets with different thickness

板厚 w/mm	焊接压力 F/kN	焊接电流 I/kA	焊接时间 t_W/周波	保持时间 t_H/周波
1.4	4.3	4.5~8.5	18	4
1.8	5.4	9~12	21	4

对于 1.4 mm厚 DP600钢板, 随着焊接电流的增加, 在进行焊后拉剪试验时, 出现不同的失效模式, 从界面撕裂模式到临界失效模式, 再到熔核剥离模式, 选取三种不同失效模式的焊点各一个, 进行金相试验, 测量压痕 $I\%$、熔核区与热影响区的维氏硬度 H_{FZ}, H_{HAZ}, 计算临界熔核直径 d_{cr}, 并与实际熔核直径 d进行对比, 计算直径比 η, 如表 2所示. 由此可见, 当熔核直径比 $\eta<1$时, 即实际熔核直径 d小于临界熔核直径 d_{cr}, 发生熔核界面撕裂模式; 当 $\eta\approx1$时, 即实际熔核直径 d接近临界熔核直径 d_{cr}, 发生临界失效模式; 当 $\eta>1$时, 即实际熔核直径 d大于临界熔核直径 d_{cr}, 发生熔核剥离模式, 评价结果与试验结果相符.

表 2　1.4 mm DP600熔核参数

Table 2　Parameters of nugget for 1.4 mm DP600

编号	实际直径 d/mm	熔核区硬度 H_{FZ}/HV	热影响区硬度 H_{HAZ}/HV	硬度比 H_{HAZ}/H_{FZ}	压痕分数 I/%	临界直径 d_{Cr}/mm	直径比 $\eta=d/d_{Cr}$	失效模式
$A_{1.4}$	6.4	436	284	0.65	12.5	7.52	0.85	界面
$B_{1.4}$	7.1	429	270	0.63	15.8	7.00	1.01	临界
$C_{1.4}$	7.3	436	274	0.63	17.5	6.84	1.07	剥离

对于 1.8 mm厚 DP600钢板, 随着焊接参数增加, 焊点始终呈现界面撕裂模式, 选取三个焊点进行上述金相试验, 结果如表 3所示. 根据熔核直径比 η计算可知, 评价结果与试验相符. 此外, 可以看出随着焊接电流的增加, 实际熔核直径 d趋于稳定, 只有降低 d_{cr}才可能出现熔核剥离模式, 而硬度比 H_{FZ}/H_{HAZ}呈上升的趋势, 由式 (9)可知, 只有增大压痕, 才可能使临界熔核直径 d_{cr}降低, 以达到熔核剥离的效果, 但过深的压痕在实际生产中是不被接受的, 因此其失效模式始终为界面撕裂.

为了实现对实际生产线上双相钢焊点失效模式的评价, 需测量压痕值 $I\%$, 板厚 t, 以及熔核区与热影响区的维氏硬度 H_{FZ}, H_{HAZ}. 由于后二者需要借助维氏硬度计, 且无法实施在线测量, 故参考文献 [10], 对试验设计中总共 31组热镀锌 DP600焊点的 H_{FZ}, H_{HAZ}进行统计, 取其平均值为 434.89 HV,

表 3　1.8 mm DP600 熔核参数

Table 3　Parameters of nugget for 1.8 mm DP600

编号	实际直径 d/mm	熔核区硬度 H_{FZ}/HV	热影响区硬度 H_{HAZ}/HV	硬度比 H_{HAZ}/H_{FZ}	压痕分数 I/(%)	临界直径 d_{Cr}/mm	直径比 $\eta=d/d_{Cr}$	失效模式
$A_{1.8}$	7.4	464	300	0.65	21.0	8.66	0.85	界面
$B_{1.8}$	7.6	465	306	0.66	25.0	8.37	0.91	界面
$C_{1.8}$	7.5	454	313	0.69	29.0	8.30	0.90	界面

263.66 HV，则 d_{Cr} 可近似为

$$d_{Cr}=5.7\times(1-I\%)t \tag{12}$$

由于压痕分数 I% 可以在线测量，该公式可近似作为实际生产中不同板厚双相钢 DP600 的焊点质量评价指标，以取代传统的熔核直径评价标准 $d=4\sqrt{t}$.

4　结　论

(1) 文中通过对双相钢焊点受载进行建模分析，计算了焊点不同失效模式下所能承受的极限载荷，进而获得了临界失效模式的熔核直径指标，经试验验证，该模型能够有效评价双相钢 DP600 焊点的失效模式.

(2) 通过对上述模型中难以在线测量的熔核区与热影响区的维氏硬度 H_{FZ}，H_{HAZ} 进行近似，获得了简化的熔核直径评价指标 $d_{Cr}=5.7\times(1-I\%)t$，可以用来代替传统的熔核直径指标 $d=4\sqrt{t}$ 解决实际生产中双相钢焊点失效模式的评价问题.

参考文献:

[1] 常方奎，孙广建. 轿车车身结构的轻量化设计[EB/OL]. (2006-11-29)[2010-10-10]. http://www.paper.edu.cn/index.php/default/releasepaper/contant/200611-823

[2] Akihiro Nishimoto, Yoshihiro Hosoya, Kazuhide Nakaoka. New type of dual-phase steel sheet for automobile outer body panels[J]. Transactions of the Iron and Steel Institute of Japan, 1981, 21(11): 778-782

[3] Shi M F, Thomas G H, Chen M X, et al. Formability performance comparison between dual phase and HSLA steels[J]. Iron and Steelmaker, 2002, 29(3): 27-32

[4] Marya M, Gayden X Q. Development of requirements for resistance spot welding dual-phase (DP600) steels part 2 — statistical analyses and process maps[J]. Welding Journal, 2005, 84(12): 197-207.

[5] Salvini P, Vullo V, Vivio F, et al. One shot failure modes in spot welded structures[J]. Welding International, 2005, 19(4): 297-304

[6] Marya M, Wang K, Hector L G, et al. Tensile-shear forces and fracture modes in single and multiple weld specimens in dual-phase steels[J]. Journal of Manufacturing Science and Engineering, 2006, 128(1): 287-298

[7] Chuko W L, Gould J E. Development of appropriate resistance spot welding practice for transformation-hardened steels[J]. Welding Journal, 2002, 81(1): 1-7.

[8] Sun X, Stephens E V, Davies R W, et al. Effects of fusion zone size on failure modes and static strength of aluminum resistance spot welds[J]. Welding Journal, 2004, 83(11): 308-318

[9] Cahoon J R, Broughton W H, Kutzak A R. Determination of yield strength from hardness measurements[J]. Metallurgical Transactions, 1971, 2(7): 1979-1983

[10] 张小云. 双相钢点焊熔核界面撕裂失效机理与控制方法研究[D]. 上海: 上海交通大学, 2008

作者简介：杨海军，男，1978 年出生，博士研究生. 主要研究车身制造技术，已发表论文 4 篇. Email: yanghaijuncn@yahoo.cn

通讯作者：张延松，男，副教授. Email: zhangyansong@sjtu.edu.cn

my Chief Equipment Ministry Laboratory of Material Interface, China University of Petroleum, Dongying 257061, China). P53－56

Abstract: By using diffusion couple made by inlaying, the diffusion layer of Al/Mg was researched under different anneal condition. The microstructure and forming rule were observed and analyzed by means of scanning electron microscopy (SEM) and Energy Disperse Spectroscopy (EDS), and its forming mechanism was discussed. The results showed that the diffusion layer was formed at Al/Mg interphase with heating temperature of 580 ℃ and holding time of 60 hours, its thickness was 265 μm, its structure was Al/Mg$_2$Al$_3$/MgAl/Mg$_3$Al$_2$/Mg which included all phases in Al/Mg binary alloy phase diagram, and the structure was consistent with the sequence of each phase located Al/Mg phase diagram. The solid phase diffusion, dissolve and crystal of Al and Mg resulted in forming of diffusion layer with different diffusion temperature and time, and the diffusion layer was almost formed at Al/Mg interphace at the same time, which was different number of layer, thickness and structure.

Key words: Al; Mg; diffusion layer; dissolve; crystal

Analysis of microstructure and binding ability of gradient coatings in controlled atmosphere DONG Xiaoqiang, LUO Chao, LI Deyuan, DUAN Sihua (School of Materials Science and Engineering, Shenyang University of Technology, Shenyang 110178, China). P57－60

Abstract: Because ceramic gradient coating with excellent performance will be affected by air oxidation effects in air atmosphere plasma spray coating preparation, NiCrBSi/Al$_2$O$_3$ gradient coating is prepared in controlled atmosphere (argon) plasma spraying. The atmospheric conditions of making NiCrBSi/Al$_2$O$_3$ gradient coatings are compared, and the effects of argon atmosphere on the microstructure and bonding strength of sprayed gradient coating are analyzed. The results show that the inside organization of gradient coating in argon atmospheres and in air has no obvious interface and achieves continuous change of microstructure, but the gradient coating organization in argon is more dense, lower oxidative and has higher bonding strength than that in air.

Key words: controlled atmosphere; plasma spraying; Al$_2$O$_3$ ceramic; gradient coatings; bond strength

Evaluation on interfacial fracture mode of resistance spot weld dual-phase steels YANG Haijun[1], ZHANG Yansong[1], LAI Xinmin[1], ZHANG Xiaoyun[2] (1. School of Mechanical Engineering, Shanghai Jiaotong University, Shanghai 200240, China; 2. Vehicle Manufacturing Engineering, Shanghai General Motors, Shanghai 201201, China). P61－64

Abstract: The interfacial fracture mode of dual phase steel (DP) weld greatly affects its mechanical performance and decreases its weld quality because much martensite in the nugget makes the welds brittle, but the traditional nugget diameter criteria is not suitable to estimate the quality of DP weld, and so this paper builds a mathematical mode based on macro-appearance and micro-mechanism to evaluate the different fracture modes of DP weld. Experimental results show that the model is effective on 1.4 mm and 1.8 mm DP600 welds and is also better than other evaluation criteria for their limited factors considered.

Key words: dual phase steel; resistance spot welding; interfacial fracture; evaluation model

Theory and experimental research on controlling crack in double-scanning laser cladding process CHEN Lie, XIE Peilin (Department of Mechanical Engineering, Naval University of Engineering, Wuhan 430033, China). P65－68

Abstract: A new craft of laser cladding unidirectional powder feeding and double scanning was developed to solve the problem of cracking in the cladding coats. The temperature field and stress field of laser cladding were computed. The results indicate that the value of stress is very large and the stress concentration problem is serious at the top of cladding coat and the joint between coat and base material in the process of unidirectional scanning. After the second scanning, the value of stress can be decreased and the stress concentrated at the top of cladding coat can be eliminated. The results of laser cladding 45 steel with Ni60 alloy powder by the craft of unidirectional powder feeding and double scanning show that the cracking of the coats can be avoided both in single-pass cladding and multi-pass lap cladding by the craft, which is effective and feasible for controlling crack in laser cladding.

Key words: laser technique; laser cladding; temperature field; stress field; stress concentration

Overlap model of interval bead based on GMAW forming MENG Fanjun, ZHU Sheng, BA Dema, DU Wenbo (Department of Equipment Remanufacturing Engineering, The Academy of Armored Forces Engineering, Beijing 100072, China). P69－71

Abstract: The lap amount of bead is critical not only for the trouble-free operation of three-dimensional welding, but also for the forming accuracy. So the interval bead lap model of the GMAW welding is established on the basis of the physical characteristics of droplet transition. Furthermore, the theoretical bead distance of flat overlaying welding layer is calculated. Actual welding test is employed for the model verification and the height of surfacing layer also is calculated. The test results agree well with the theoretical ones, which establish the foundation for the welding automation.

Key words: three-dimensional welding; interval welding; lap amount of bead; overlaying welding layer

Analysis of intersection surface welding motion simulation based on Pro/Engineer WANG Xinhui, YU Dan, YANG Kefei, MENG Zhaolin (Harbin Welding Institute, China Academy of Machinery Science & Technology, Harbin 150080, China). P72－76

Abstract: In the development process of automatic welding equipment which is used for the complex inner surface welding in petroleum drill special-purpose valve, the mathematic model of valve inner surface intersection curve was modeled, and